2-20-2007

The Resolved Stellar Populations of a Dwarf Spheroidal Galaxy in the Virgo Cluster

Patrick R. Durell
Youngstown State University, prdurrell@ysu.edu

Ted von Hippel
University of Texas at Austin, vonhippt@erau.edu

et al.

The Astrophysical Journal, 656:746–755, 2007 February 20

THE RESOLVED STELLAR POPULATIONS OF A DWARF SPHEROIDAL GALAXY IN THE VIRGO CLUSTER

Patrick R. Durrell,[1] Benjamin F. Williams,[2] Robin Ciardullo,[2] John J. Feldmeier,[1,3] Ted von Hippel,[4] Steinn Sigurdsson,[2] George H. Jacoby,[5] Henry C. Ferguson,[6] Nial R. Tanvir,[7] Magda Arnaboldi,[8] Ortwin Gerhard,[9] J. Alfonso L. Aguerri,[10] Ken Freeman,[11] and Matt Vinciguerra[2]

Received 2006 September 25; accepted 2006 November 1

ABSTRACT

We report on the discovery of a faint ($M_V \sim -10.6 \pm 0.2$) dwarf spheroidal galaxy on deep F606W and F814W *Hubble Space Telescope* images of a Virgo intracluster field. The galaxy is easily resolved in our images, as our color magnitude diagram (CMD) extends $\gtrsim$1 magnitude beyond the tip of the red giant branch (RGB). Thus, it is the deepest CMD for a small dwarf galaxy inside a cluster environment. Using the colors of the RGB stars, we derive a metal abundance for the dwarf of $[\mathrm{M/H}] = -2.3 \pm 0.3$ and show that the metallicity dispersion is less than 0.6 dex at 95% confidence. We also use the galaxy's lack of AGB stars and the absence of objects brighter than $M_{\mathrm{bol}} \sim -4.1 \pm 0.2$ to show that the system is old ($t \gtrsim 10$ Gyr). Finally, we derive the object's structural parameters and show that the galaxy displays no obvious evidence of tidal threshing. Since the tip of the red giant branch distance [$(m - M)_0 = 31.23 \pm 0.17$ or $D = 17.6 \pm 1.4$ Mpc] puts the galaxy near the core of the Virgo cluster, one might expect the object to have undergone some tidal processing. Yet the chemical and morphological similarity between the dwarf and the dSph galaxies of the Local and M81 Group demonstrates that the object is indeed pristine and not the shredded remains of a much larger galaxy. We discuss the possible origins of this galaxy and suggest that it is just now falling into Virgo for the first time.

Subject headings: galaxies: abundances — galaxies: clusters: individual (Virgo) — galaxies: dwarf — galaxies: stellar content

1. INTRODUCTION

An understanding of the processes that affect the formation, evolution, and sometimes destruction of dwarf galaxies is critical to our overall picture of galaxy formation. Since dwarf galaxies are the most common type of galaxy in the universe, any model of galaxy formation is incomplete if we cannot understand these objects. Moreover, under the current paradigm of hierarchical structure formation (e.g., Kauffmann et al. 1993; Cole et al. 2000), massive galaxies are formed from the mergers of less massive objects. Thus, dwarf galaxies are an important building block of the universe, and an understanding of their properties will help illuminate the processes of galaxy formation more generally.

The faintest examples of dwarf galaxies are the dwarf spheroidals (dSphs). Using the nomenclature of Grebel et al. (2003), these are low-luminosity ($M_V \gtrsim -14$), low central surface brightness ($\mu_V \gtrsim 22$ mag arcsec^{-2}) objects with shallow radial profiles and stellar populations that are dominated by old and intermediate-aged stars.[12] Most of what we know about dSphs comes from observations of $\sim$20 galaxies in the low-density environment of the Local Group. From the data, it appears that dSphs are fairly homogeneous in nature, with small, but dense dark matter halos and low metallicities that are in proportion to their luminosity (for a review see Mateo 1998).

Much less is known about dSphs in the cluster environment. Surveys in Virgo and Fornax have successfully found large numbers of dE and bright dSph galaxies (Binggeli et al. 1985; Ferguson 1989; Phillipps et al. 1998; Trentham & Hodgkin 2002; Sabatini et al. 2003), but there is still considerable uncertainty as to just how many of these lowest luminosity objects exist (e.g., Hilker et al. 2003). The scarce information we do have on cluster dSph galaxies suggests that their properties are similar to those of Local Group dwarfs (Hilker et al. 2005; Caldwell 2006). If correct, then such a result is somewhat surprising, since the tidal forces of the cluster environment are expected to take their toll on these objects. Indeed, Bekki et al. (2001) have shown that dSphs can be stripped of their outer stars in only a few Gyr. This would imply that both the morphology and chemistry of cluster dSphs should differ significantly from their Local Group counterparts.

Until recently, abundance studies of cluster dSph galaxies (based on photometry of individual stars) have been impractical. For example, although Harris et al. (1998) were able to resolve the brightest red giant branch (RGB) stars in a Virgo cluster dE,N galaxy using a 32 ks exposure with the *Hubble Space Telescope*'s Wide Field Planetary Camera 2 (WFPC2), these data were limited to a single filter (F814W). However, with the advent of the Advanced Camera for Surveys (ACS), it is now possible to measure the broadband colors of red giants in these systems. Indeed, Caldwell (2006) has recently used the ACS to resolve the stellar

[1] Department of Physics and Astronomy, Youngstown State University, Youngstown, OH; prdurrell@ysu.edu, jjfeldmeier@ysu.edu.
[2] Department of Astronomy and Astrophysics, Pennsylvania State University, University Park, PA; bwilliams@astro.psu.edu, rbc@astro.psu.edu, steinn@astro.psu.edu.
[3] NSF Astronomy and Astrophysics Postdoctoral Fellow.
[4] The University of Texas, Department of Astronomy, Austin, TX; ted@astro.as.utexas.edu.
[5] WIYN Observatory, Tucson, AZ; jacoby@wiyn.org.
[6] Space Telescope Science Institute, Baltimore, MD; ferguson@stsci.edu.
[7] Department of Physics and Astronomy, University of Leicester, Leicester, UK; nrt3@star.le.ac.uk.
[8] European Southern Observatory, Garching, Germany; marnabol@eso.org.
[9] Max-Planck-Institut fuer Extraterrestrische Physik, Garching, Germany; gerhard@exgal.mpe.mpg.de.
[10] Instituto de Astrofisica de Canarias, La Laguna, Tenerife, Spain; jalfonso@ll.iac.es.
[11] Mount Stromlo Observatory, Research School of Astronomy and Astrophysics, Mount Stromlo Observatory, Australian National University, Australia; kcf@mso.anu.edu.au.

[12] dSph galaxies are the faint end of the dwarf elliptical (dE) galaxy sequence, and when we note dE galaxies we are including those gas-poor dwarf galaxies more luminous than $M_V = -14$.

populations of four dE/dSph galaxies in the Virgo cluster and obtain color-magnitude diagrams (CMDs) of their stars down to $I \sim 28$, making it the deepest study of individual stars in cluster dwarf galaxies. Their data appear to confirm that the dE/dSph galaxies of Virgo obey the same luminosity-metallicity relation as the dE/dSph galaxies of the Local Group.

Here, we present an extremely deep F606W and F814W study of a faint ($M_V \sim -10.6$) dSph that was serendipitously found during a survey of intracluster stars in Virgo (Williams et al. 2007a). We use the data, which reach $I \sim 28.4$, to show that the galaxy is remarkably similar to undisturbed dSphs in the Local Group, in both morphology and stellar content. In § 2, we describe both our data reductions and our artificial star experiments and present a color-magnitude diagram of the dSph's red giant branch stars. In § 3, we use these data to derive the system's distance, as well as its stellar population. We show that the galaxy has a mean metallicity that is very low ($[M/H] \sim -2.3 \pm 0.3$) and is composed entirely of stars older than 8–10 Gyr. We also derive the galaxy's structural parameters and show that its central surface brightness and core radius are typical of dSphs in the Local Group. In § 4, we compare the galaxy's properties to those of Local Group objects and attempt to investigate the effects of environment on its history. We show that the galaxy displays no obvious evidence of tidal disruption and has a mean metallicity appropriate for its luminosity. We conclude by considering the possible origin of this object.

2. OBSERVATIONS AND DATA ANALYSIS

Between 2005 May 30 and 2005 June 7 we used the Advanced Camera for Surveys on the *Hubble Space Telescope* to obtain deep F606W and F814W images of a Virgo intracluster field [$\alpha(2000) = 12^h28^m10.80^s$, $\delta(2000) = 12°33'20.0''$, orientation 112.58°]. This field, which is projected ~180 kpc from M87 (assuming a mean Virgo distance $d = 16$ Mpc; e.g., Jerjen et al. 2004), was chosen to be near the cluster center, but away from any known object; the closest cataloged galaxy is the dwarf elliptical VCC 1051, which is ~5′ (24 kpc) to the northwest; the nearest large galaxy, M86, is over 170 kpc away.

Our F814W (*I*-band) data consisted of 22 exposures with 26,880 s of integration time; the F606W (wide *V*-band) observation included 52 exposures totaling 63,440 s. These data were co-added and resampled using the MultiDrizzle[13] task within PyRAF[14] (Koekemoer et al. 2002) to produce images with $0.03''$ pixel^{-1}. The details of these reductions, and an image of the field illustrating its position in the cluster is given by Williams et al. (2007a).

Immediately after data acquisition, an inspection of our images revealed the presence of a previously unknown galaxy in the field. The object, whose center is located at $\alpha(2000) = 12^h28^m15.5^s$, $\delta(2000) = +12°33'37.0''$ (uncertainty ~$0.2''$) is ~$15''$ in extent and clearly resolved into stars. A color image of the object is shown in Figure 1.

Our point source photometry was similar (but not identical to) that performed by Williams et al. (2007a). To avoid dealing with variations in the ACS point-spread function (PSF), we began by limiting our photometric reductions to a 2200×1600 pixel ($66'' \times 48''$) region surrounding the galaxy. We then chose three bright, isolated stars on our F606W image and four bright isolated stars on the F814W image to define the PSFs and used

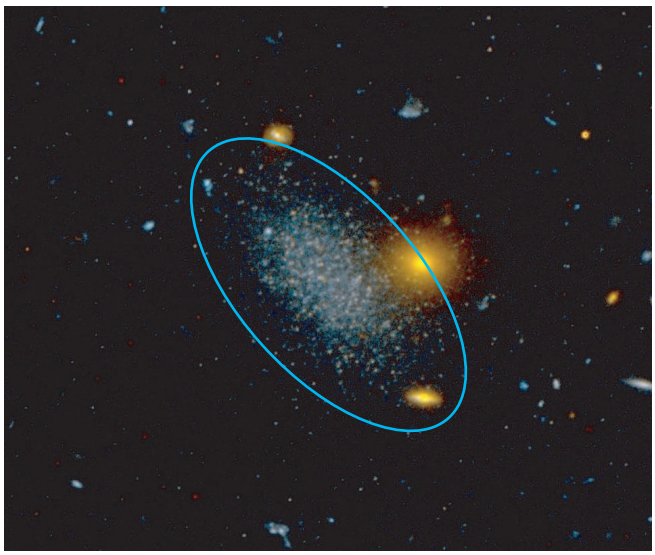

FIG. 1.—Color image of a $28'' \times 24''$ section of our image, centered on the dSph galaxy. In the image, blue represents 2(F606W − F814W), green represents F606W, and red represents F814W. The ellipse denotes the boundary used to defined a subsample of stars that minimizes contamination (see text). North is to the top, and east is to the left.

DAOPHOT II and ALLSTAR to perform the photometry (Stetson 1987, 1992). Two DAOPHOT II/ALLSTAR passes were performed to detect as many of the stars as possible. The F606W and F814W data sets were then merged with a 1.5 pixel matching criterion to create a preliminary object catalog of ~1000 objects. Finally, we used the DAOPHOT χ and r_{-2} image parameters to remove background galaxies and severely blended stars from the list (Stetson 1987; Kron 1980).

Our instrumental magnitudes were placed on the Vegamag system using the prescription and zero points provided by Sirianni et al. (2005). To obtain the offset between our ALLSTAR magnitudes and the Vegamag system, we used the profiles of the PSF stars on each image; the rms scatter in this calibration was ~0.02 mag. We note that since the region under consideration is small (only ~8% of the entire ACS field), differential effects associated with charge transfer efficiency were negligible (~0.01–0.02 mag) and were ignored.

2.1. *Artificial Star Experiments*

To ascertain the photometric uncertainties and incompleteness in our data, we used the traditional method of adding simulated stars of known brightness to the science frames and rereducing them following the exact same procedures as for the original data. To each frame, we added 9000 stars (300 runs with 30 stars added per run) to an elliptical region centered on the dwarf galaxy and reexecuted our two-pass DAOPHOT II/ALLSTAR photometric procedure, including the rejection of nonstellar sources and the merging of the data sets. By limiting the number of fake stars to 30 per run, we did not significantly alter the crowding conditions on the images; by defining the mean F606W − F814W color of our artificial stars to be roughly equal to that of the observed objects (F606W − F814W = 1.0), we ensured that our experiments adequately reproduced losses during the catalog merging and image classification processes. Finally, by defining the stars' luminosity function to be a rising exponential between F814W = 22 and 29, we improved our statistics at the faint end of the luminosity function, where the uncertainties are largest. The result of these experiments were the photometric completeness function

[13] MultiDrizzle is a product of the Space Telescope Science Institute, which is operated by AURA for NASA: http://stsdas.stsci.edu/pydrizzle/multidrizzle.

[14] PyRAF is a product of the Space Telescope Science Institute, which is operated by AURA for NASA.

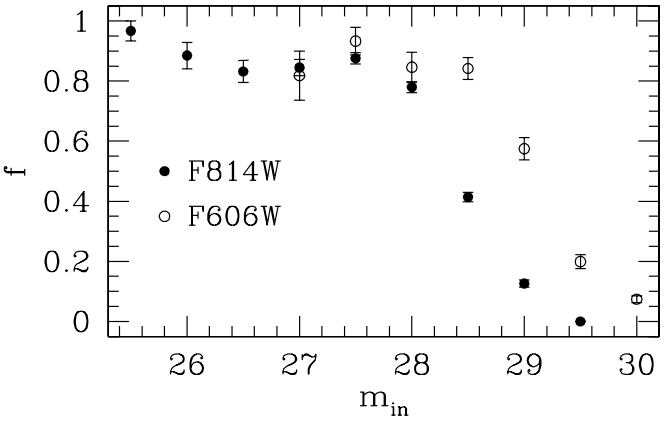

FIG. 2.—Fraction f of recovered artificial stars for the F814W (*filled circles*) and the F606W (*open circles*) images. The F606W data is based on added stars with input colors F606W − F814W = 2.0 and that of the F814W data is from stars with input colors F606W − F814W = 0.0.

$f(m)$, defined as the ratio of the stars recovered to stars added *regardless of the magnitude that was actually measured*; $\Delta(m)$, the mean shift in magnitude of the stars [$\Delta(m) = m_{\rm out} - m_{\rm in}$]; and $\sigma(m)$, the dispersion about this mean. All of these functions were computed in 0.5 mag bins, to ease the computational requirements.

To ascertain each filter's limiting magnitude (defined as the 50% completeness fraction), we performed similar artificial star tests using a variety of F606W − F814W input colors. The results from these experiments are illustrated in Figure 2. From these experiments, we obtained $m_{\rm lim} = 29.1 \pm 0.1$ in F606W and 28.4 ± 0.1 in F814W, where the errors reflect both the rms scatter due to the use of different colors and the uncertainty associated with varying levels of crowding within the galaxy. As expected, these limits are slightly brighter than those found by Williams et al. (2007a), whose analysis focused on the uncrowded regions of the frame. Moreover, our classification criteria kept only those objects with the best photometric accuracy; obvious galaxies and extremely blended objects were removed from the catalog. As result, even at F814W = 27, ∼10% of the artificial stars were not recovered. Fortunately, since we are not making any inferences based solely on the absolute number of stars detected, these missing objects do not affect our analyses in any significant way.

A color-magnitude diagram for our artificial stars is shown in Figure 3. The figure illustrates that the photometric errors increase with magnitude, so that by $m_{\rm lim}$, the uncertainties are ∼0.2 mag. The figure also shows that there is a small blueward shift at faintest levels; this is due to the uneven depth of the two images. (At the faintest levels, our F814W photometry only detects objects whose photometric errors are in the positive direction.) Fortunately, down to the limiting magnitudes of the frames, this color shift is <0.1 mag. These corrections, while small, will be accounted for in the following sections.

2.2. *Color Magnitude Diagram*

The color-magnitude diagram for all the stellar objects in our field is displayed in the left-hand panel of Figure 4. The diagram shows that most objects lie in a sequence near F606W − F814W ∼ 1 that extends up to F814W ∼ 27.1. However, there is a significant amount of scatter about this line. This scatter comes from two sources: the RGB stars that pervade Virgo's intracluster space (Ferguson et al. 1998; Durrell et al. 2002; Williams et al. 2007a) and, to a lesser extent, unresolved background galaxies. To minimize the effects of these contaminants,

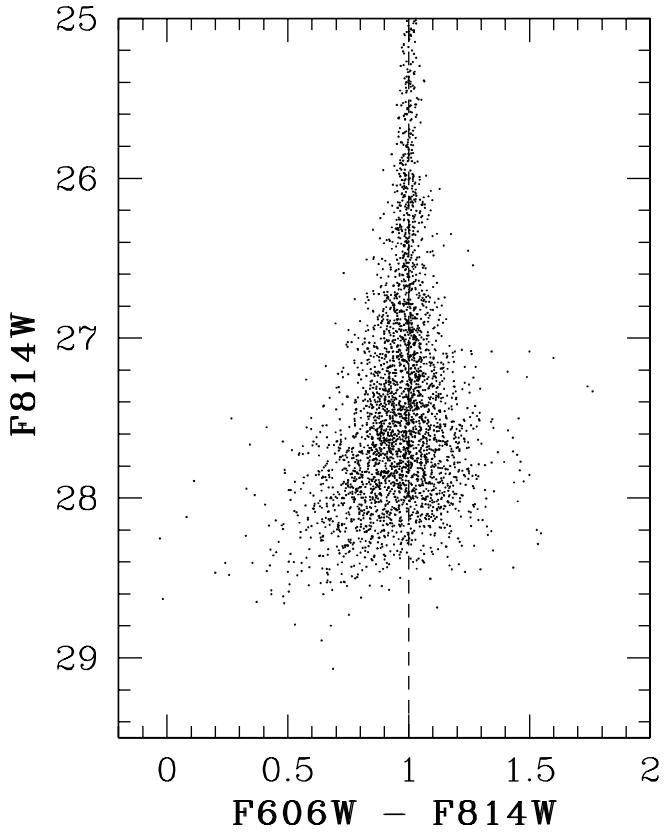

FIG. 3.—Output color-magnitude diagram for our artificial stars. The dashed line denotes the input colors for the stars F606W − F814W = 1.00. Note the slight offset in the colors at faint magnitudes. This is due to the different limiting magnitudes of the two filters.

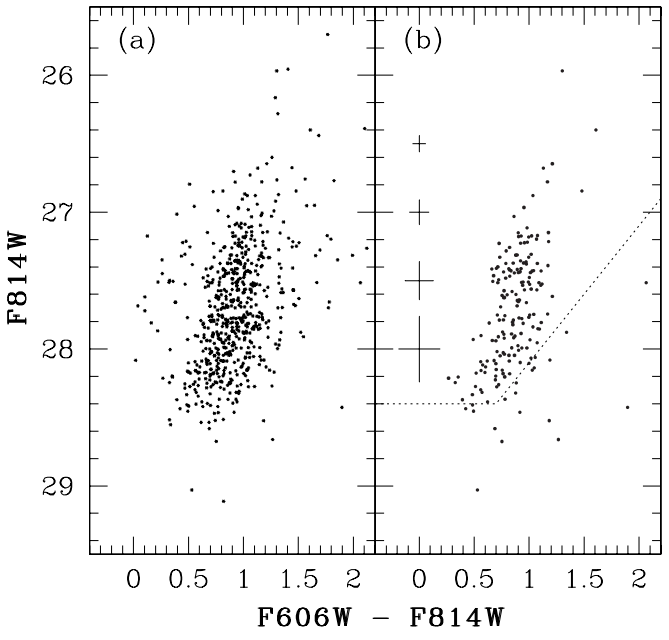

FIG. 4.—(*a*) Color-magnitude diagram (in the Vegamag system) for the 611 stellar objects located in a $66'' \times 48''$ region centered on the dSph galaxy. (*b*) The "dwarf-only" CMD, formed from a subset of 181 stars located within the inner elliptical region shown in Fig. 1. The dotted lines denote the 50% completeness levels, while the error bars represent the typical photometric uncertainties. Note the discontinuity at F814W ∼ 27.1; this is the tip of the red giant branch.

we identified a subsample of stars within the galaxy's F814W $\sim$ 26.5 mag arcsec^{-2} isophote. This subsample, which is defined via an ellipse with semimajor axis 8.1″, an axis ratio of $b/a = 0.5$, and a position angle of 43° (see § 3.4) should have minimal contamination; based on star counts in the rest of our field, only $\sim$16 out of the 171 objects brighter than F814W = 28.4 should be contaminants. Thus, we can use the data from this 103 arcsec^2 region to form a "clean" color-magnitude diagram of the galaxy's stars. The elliptical region that defines our subsample is shown in Figure 1; the right-hand panel of Figure 4 shows its CMD.

3. ANALYSIS

The CMD in Figure 4 displays the hallmarks of a red giant branch population with F814W > 27. There are few stars brighter than this limit, and no evidence of any bright blue stars arising from a young stellar population. Since the data clearly extend more than 1 mag down the RGB, we can use the diagram to investigate both the distance and metallicity of the galaxy.

3.1. *TRGB Distance*

The tip of the red giant branch (TRGB) in the *I* band has repeatedly been shown to be an excellent distance indicator for old, metal-poor populations. In stellar systems with [M/H] < -1, the TRGB is essentially independent of both age and metallicity (e.g., Lee et al. 1993; Sakai et al. 1996; Ferrarese et al. 2000; Bellazzini et al. 2001; McConnachie et al. 2004; Mouchine et al. 2005; Caldwell 2006), so all that is required is a measure of the bright-end truncation of the RGB and an estimate of foreground reddening [$E(B-V) = 0.025$; Schlegel et al. 1998]. Our only limitation is the small size of the galaxy, which restricts the number of stars available for analysis.

Although foreground/background contamination in our "dwarf-only" CMD (right panel of Fig. 4) is small, to make our TRGB detection as unambiguous as possible, we have further restricted our sample to objects with F606W − F814W < 1.3. Stars redder than this are not on the metal-poor RGB and are unlikely to be members of the galaxy. This makes very little difference to the analysis, since it excludes only 3 objects from consideration. Moreover, since the RGB tip for red, metal-rich stars is fainter than that for blue objects, eliminating these stars should not affect our distance determination. We note that the ACS F814W filter bandpass is very similar to that of the traditional *I* band; according to Sirianni et al. (2005), the transformation between these two systems is $I = \mathrm{F814W} - 0.008$ (for stars with F606W − F814W = 1) in the Vegamag system.

Visual inspection of the Figure 4 shows a rather sharp transition at F814W $\sim I \sim 27.1$, albeit with a small number of stars. While the increased Poissonian noise from small numbers can lead to a possible systematic bias in I_{TRGB}, Madore & Freedman (1995) have shown that with at least $\sim$100 stars in the top magnitude of the RGB, such biases are small. Since our analysis includes $\sim$130 objects, we are safely above this threshold.

Another possible source of systematic error is image crowding; in dense fields, stellar blends can make the RGB tip appear brighter than it should be. However, in our case, this effect should not be important. Our artificial star experiments demonstrate that the mean magnitude shift at F814W ~ 27 is very small, less than 0.01 mag. This result, which is confirmed by additional artificial star experiments with F814W < 27.1, is due principally to our image classification criteria, which rejects the most heavily blended objects (i.e., those most likely to bias the results toward brighter magnitudes).

A quantitative estimate of the RGB tip location can be derived using the Sobel edge-detection filter of Lee et al. (1993).

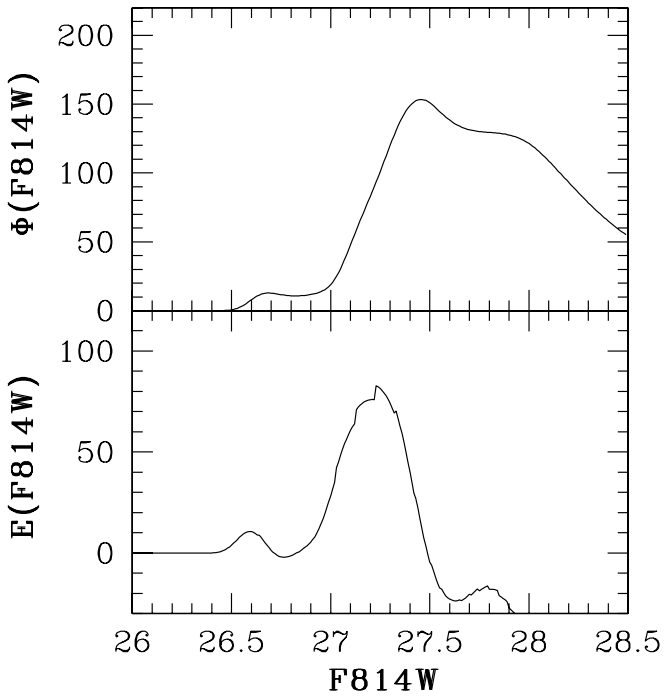

FIG. 5.—*Top*: Continuous luminosity function formed by co-adding the Gaussian representation of stars in our minimally contaminated subsample (see text). Objects with F606W − F814W > 1.3 have been excluded from the analysis. *Bottom*: Result of applying the Sobel edge-detection algorithm. This panel suggests that the tip of the red giant branch is at $\mathrm{F814W}_{\mathrm{TRGB}} = 27.22 \pm 0.15$.

This technique, which was originally used on binned functions, has since been modified to work on discrete stellar samples by treating each object as a Gaussian distribution with a dispersion equal to the expected photometric error (Sakai et al. 1996). We note that more rigorous techniques have been employed to derive I_{TRGB}, such as the method of maximum likelihood (Méndez et al. 2002; Mouhcine et al. 2005) and the second derivative of the luminosity function (Cioni et al. 2000). However, maximum likelihood methods are better for data sets where the RGB power-law slope is observed for over a magnitude. In our case, photometric incompleteness and image crowding make the use of the technique problematic. Moreover, the small number of stars limits the reliability of second derivative calculations. Because our background contamination is so small, the simpler Sobel edge-detection filter should be adequate for our purpose.

To employ the Sobel-edge detection method, we treated each star as a Gaussian distribution with a mean equal to its observed magnitude (plus the small Δm shift predicted by our artificial star experiments) and a dispersion, $\sigma(m)$, equal to the photometric uncertainty at that magnitude. We then co-added the Gaussians to produce the luminosity function shown in the top panel of Figure 5. Even with the large photometric errors ($\sigma \sim 0.07$ at F814W = 27), the sharp rise of the luminosity function is evident, as is a small contribution from brighter stars, which presumably arise from the galaxy's AGB component (more on this below).

To determine the location of the tip of the red giant branch, we applied to our continuous luminosity function the edge-detection algorithm

$$E(m) = \Phi(m + \sigma(m)) - \Phi(m - \sigma(m)), \qquad (1)$$

where $\sigma(m)$ is the photometric error defined via our artificial star experiments (Sakai et al. 1996). This function, which is displayed in the bottom panel of Figure 5, reveals a rather wide peak near

F814W $\sim$ 27.2. From the figure, the location of the RGB discontinuity is at $I_{\rm TRGB} = 27.22 \pm 0.15$, where the uncertainty is based on the full-width at half-maximum of the distribution. This error is likely conservative (e.g., Sakai et al. 1996), although it is similar to that expected based on the number of stars available (Madore & Freedman 1995).

To derive the distance to the dwarf, we adopt $M_{I,\rm TRGB} = -4.06 \pm 0.07$ (random error) as the absolute magnitude of the metal-poor RGB tip (Ferrarese et al. 2000). This number is very similar to that of other recent determinations: the empirical calibration of Da Costa & Armandroff (1990) yields $M_{I,\rm TRGB} = -3.96 \pm 0.06$ for objects with [Fe/H] $= -2.3$, while a more recent determination by Bellazzini et al. (2001) gives $M_{I,\rm TRGB} = -4.04 \pm 0.12$ for [Fe/H] $= -1.7$. (The metallicity dependence of $M_{I,\rm TRGB}$ over this range is much smaller than these random errors.) Thus, we derive $(m - M)_I = 31.28 \pm 0.17$ for the dwarf. Assuming a foreground reddening of $E(B - V) = 0.025$ (Schlegel et al. 1998) (and thus $A_{\rm F814W} \sim A_I = 0.046$; Sirianni et al. 2005), we derive a distance modulus of $(m - M)_0 = 31.23 \pm 0.17$, or $D = 17.6 \pm 1.4$ Mpc (random error only). This distance is similar to the Cepheid, surface brightness fluctuation, and planetary nebula luminosity function distances to the core of Virgo (Jacoby et al. 1990; Freedman et al. 2001; Tonry et al. 2001). Although the three-dimensional structure of the Virgo cluster is complex, the line-of-sight depth of the Virgo core (as defined by the early-type galaxies) surrounding M87 is at least $\sim$2–3 Mpc (e.g., Neilsen & Tsvetanov 2000; Jerjen et al. 2004), and the distance to the object is consistent with being located near the center of the cluster.

3.2. *Metallicity*

As noted earlier, much of the color spread in the dSph's RGB is due to photometric errors. Thus, to measure metallicity, our approach was to derive a *mean* abundance for the galaxy and then attribute any additional scatter on the RGB to a dispersion in metallicity. Since the preceding analysis has shown that the galaxy contains no significant AGB population (also see § 3.3), we can ignore the alternative that the color spread is due to the presence of young or intermediate-age stars.

To derive the mean metallicity of the dSph galaxy, we compared the ridge line derived from the CMD in Figure 4 with the scaled solar abundance isochrones of L. Girardi (2005, private communication), which are the Padova isochrones (Girardi et al. 2000, 2002) transformed directly to the ACS WFC filter system. In addition, we have also used the observed fiducial sequences from Brown et al. (2005) that are derived from photometry of Milky Way clusters covering a wide range in metallicity. Figure 6 compares the L. Girardi (2005, private communication) 12.5 Gyr sequence [shifted by $(m - M)_{\rm F814W} = 31.29$ and E(F606W − F814W) $= 0.025$] to the observed colors of the galaxy's RGB stars, both with and without the Δm magnitude shifts predicted by our artificial star experiments. Also shown for comparison is the M92 fiducial sequence of Brown et al. (2005). According to Brown et al. (2005), this cluster has an [Fe/H] value of -2.14, but is enhanced in α-process elements by $[\alpha/{\rm Fe}] = +0.3$, thus implying $Z \sim 0.0003$. Consequently, its position in the color-magnitude diagram is consistent with the $Z = 0.0004$ scaled solar Padova isochrone.

As Figure 6 illustrates, the dSph galaxy is extremely metal-poor; the colors of its RGB stars are bluer than the metal-poor M92 fiducial and very near the $Z = 0.0001$ Padova isochrone. For a more quantitative estimate, we can use the mean color of the RGB at F814W $= 27.6 \pm 0.1$ (or $M_{\rm F814W} = -3.7$ at the distance of the dwarf) and interpolate in the Padova models; this

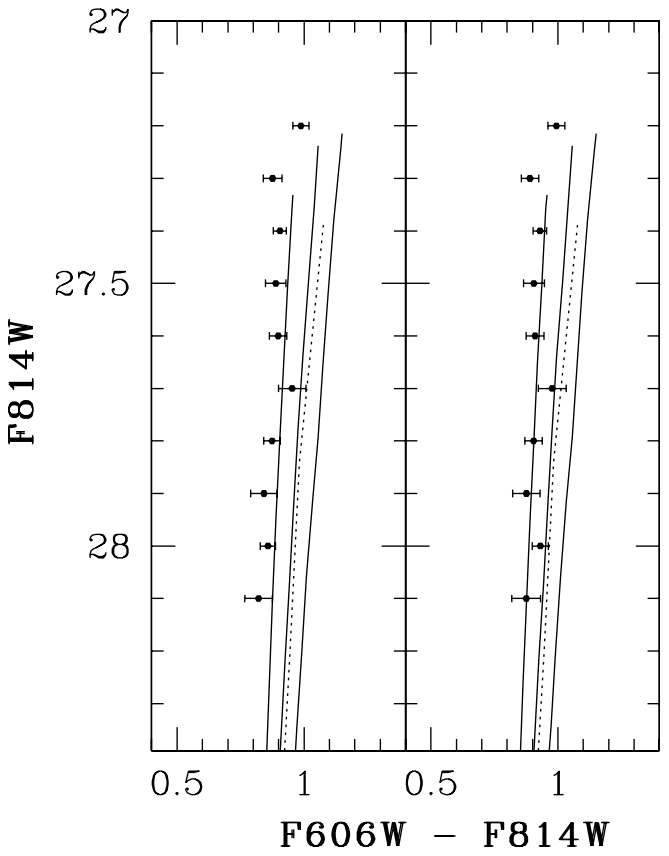

FIG. 6.—Comparison of observed red giant branch of our dSph galaxy with the 12.5 Gyr models of L. Girardi (2005, private communication). The solids are (from left to right) $Z = 0.0001$, 0.0004, and 0.001. The dashed lines show the M92 fiducial ($Z \sim 0.0003$) from Brown et al. (2005). All the curves have been shifted to a distance modulus of $(m - M)_{\rm F814W} = 31.29$ and reddened by E(F606W − F814W) $= 0.025$. The points represent the observed mean red giant branch, while the error bars show the uncertainties in the mean. The left panel displays the raw measurements; the right panel shifts the observed colors by an amount predicted by our artificial star experiments.

particular magnitude was chosen to be deep enough to adequately sample the RGB (e.g., not at the RGB tip), but not so faint as to be adversely affected by large photometric errors and photometric incompleteness. This procedure yields a mean metallicity for the system of [M/H] $= -2.3 \pm 0.3$, where the quoted error is that of the mean, not of the distribution. This error does not include possible systematic errors in the Padova models, but does include a $\pm$0.1 dex uncertainty due to distance. The errors in our color calibration ($\sim$0.03 mag) and the reddening ($\sim$0.02 mag) contribute an additional $\pm$0.3 dex uncertainty to our determination.

To estimate an upper limit to the metallicity spread in the galaxy, we compared the observed width of the RGB to the expected dispersion derived from our artificial star experiments. To do this, we used the data displayed in the right-hand panel of Figure 4, while excluding the one, extremely red (F606W − F814W $= 2.06$, F814W $= 27.5$) object from consideration. We then formed the sum

$$\chi^2 = \sum_i \frac{(c_{\rm obs} - c_{\rm iso})^2}{\sigma_c^2}, \qquad (2)$$

where $c_{\rm obs}$ is the observed F606W − F814W color of each star with $27.3 <$ F814W < 28.0, $c_{\rm iso}$ is the predicted color for the star (given its observed F814W magnitude and a system metallicity of [M/H] $= -2.3$), and σ_c is the expected color dispersion at

magnitude F814W, derived from our artificial star experiments. The resulting value, $\chi^2/\nu = 1.16$ for 95 degrees of freedom, indicates that the true red giant branch is slightly wider, but not inconsistent with, the distribution expected from a single metallicity population. This same type of analysis also demonstrates that any additional (intrinsic) color dispersion on the red giant branch must be less than $\sigma_{\rm F606W-F814W} \sim 0.09$ at the 95% confidence level. This limits the metallicity spread of our dSph galaxy to $\lesssim$0.6 dex.

3.3. *AGB Stars and the Age of the Stellar Population*

The presence of stars brighter than the RGB tip have often been used to ascertain the existence of intermediate-age ($t < 10$ Gyr) stars; the more luminous the tip of the AGB, the younger the stellar population (e.g., Mould & Aaronson 1982; Armandroff et al. 1993; Caldwell et al. 1998). Our CMD shows that our dwarf spheroidal galaxy contains very few stars brighter than F814W $\sim$ 27.1. However, since the number of stars present in the galaxy is small, it is difficult to make precise measurements of the AGB phase of evolution. Moreover, as Williams et al. (2007a) have demonstrated, our dwarf galaxy resides within a sea of intracluster stars, so any RGB stars foreground to the dwarf can masquerade as "brighter" AGB objects.

Nevertheless, it is possible to place a limit on the presence (or absence) of AGB stars in our galaxy. To do this, we used our derived distance to the dSph and the stars' observed colors to estimate the bolometric magnitudes of the galaxy's brightest objects. Specifically, we converted the stars' F606W $-$ F814W colors to $(V - I)$ using the color terms of Sirianni et al. (2005) and applied the Da Costa & Armandroff (1990) bolometric correction

$$\mathrm{BC}_I = 0.881 - 0.243(V - I)_0 \qquad (3)$$

to generate values of $M_{\rm bol}$ for all objects fainter than F814W $=$ 26.0. This procedure is uncertain at the $\sim$0.2 mag level; in addition to $\sim$0.05 mag errors associated with the color transforms and bolometric correction, our distance to the galaxy is uncertain by $\sim$0.15 mag. Nevertheless, this calculation is sufficiently accurate for our purpose.

A histogram of the derived values of $M_{\rm bol}$ for the brightest stars in the right-hand panel of Figure 4 is shown in Figure 7. Also plotted are the maximum attainable luminosities for AGB stars produced by 3, 5, 8, and 10 Gyr old populations (Rejkuba et al. 2006). As the figure illustrates, our sample of stars contains two objects that may indicate the existence of a (small) number of intermediate age objects. Both are sufficiently luminous ($\sim$0.8 and $\sim$0.4 mag brighter than the RGB tip) to exclude the possibility of image blending. However, both are also located on the very outskirts of the galaxy, where the likelihood of contamination is greatest. Since the density of intracluster stars (immediately surrounding the dwarf) with $26 <$ F814W < 27 is 36 arcmin^{-2}, we should expect our sample to contain $\sim$1 contaminating source in this magnitude range. Thus, it is uncertain whether these two bright objects are actual members of the galaxy.

Two of the three remaining stars with $-4.2 < M_{\rm bol} < -4.0$ are projected near the center of the galaxy and are thus likely to be associated with the dSph. If we apply the age-$M_{\rm bol}$ relation of Rejkuba et al. (2006) to these objects, then the inferred age of the stellar population is more than 8–10 Gyr. This is similar to the ages of the old populations seen in Local Group dSphs (Mateo 1998). We cannot exclude the possibility that these objects may be blends due to the more crowded environment; if this is indeed the case, this would strengthen the conclusion that the galaxy contains no stars with ages less than $\sim$10 Gyr.

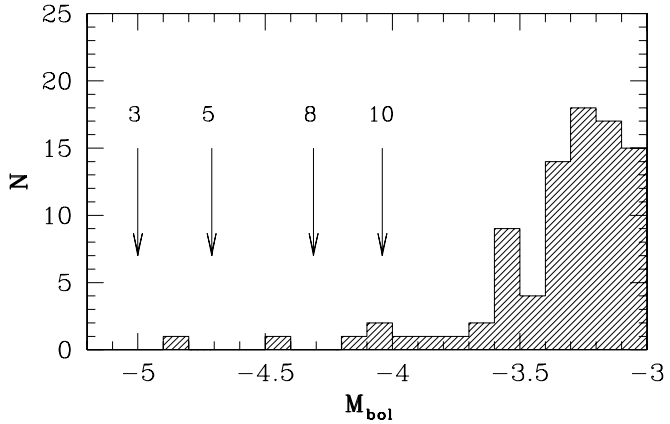

FIG. 7.—Histogram of bolometric magnitudes for the brightest stars in our minimally contaminated dSph subsample; no corrections for photometric incompleteness have been applied. The arrows denote the maximum attainable brightnesses of AGB stars formed from populations with ages of 3, 5, 8, and 10 Gyr (from Fig. 19 of Rejkuba et al. 2006). The two brightest stars are likely interlopers. The data suggest that the dSph population is at least 8 Gyr old.

3.4. *Surface Brightness Profile*

In order to determine the basic structural parameters for our dSph, we performed surface photometry on smoothed images of our frames. To do this, we began by increasing the per-pixel signal-to-noise ratio of the F606W and F814W images by rebinning the data 3×3. We then smoothed each frame with a circular Gaussian filter to produce images with a $\sim$0.6″ point-spread function and fit ellipses to the dSph's contours using the `ellipse` task in IRAF/STSDAS (Busko 1996, based on the algorithms of Jedrzejewski 1987). To facilitate these fits, the center of the galaxy was kept fixed for each contour, but the position angle and ellipticity were allowed to vary to produce the best results. In addition, to aid in the measurement of this low surface brightness object, models were also computed for three nearby background galaxies, whose light contaminates the dSph's outer contours. By subtracting these models from the original image, we were able to improve the fits for the target galaxy. Finally, to compute the surface brightness of each fitted contour, a sky background was determined using the median pixel value derived within "empty" regions of our frame. The resulting surface brightness profiles (out to a radius of 9.3″ along the major axis) are plotted in Figure 8 as a function of the geometric mean radius $[r = (ab)^{1/2}]$.

Figure 8 confirms that our galaxy is indeed a dwarf spheroidal. The central surface brightness of the galaxy is typical of Local Group dwarf spheroidals (Mateo 1998), with $\mu_0 = 24.54 \pm 0.03$ in F606W and $\mu_0 = 23.70 \pm 0.03$ in F814W. Moreover, as the dotted line in the figure demonstrates, the profile of the galaxy is well fit by a King (1962) model. To derive this line, we convolved a series of King (1962) profiles with the smoothed PSF, and fit the F814W data using all measurements with errors less than 0.3 mag. This procedure yields an excellent fit $\chi^2/\nu = 7.9/20 = 0.40$, with a core radius of $r_c = 2.6'' \pm 0.7''$ and a tidal radius of $r_t = 10'' \pm 3''$, where the uncertainties are derived via Monte Carlo simulations (see Williams et al. 2007b). At the distance of the dwarf, these measurements correspond to $r_c = 220 \pm 80$ pc and $r_t = 850 \pm 250$ pc, where the errors include the uncertainties in both the fit and the distance.

We have also fit our surface brightness profiles with the commonly used Sérsic (1968) profile (see also Graham & Driver 2005), i.e., $\Sigma = \Sigma_0 e^{-(r/r_0)^{1/n}}$. Least-squares fits to the F814W and F606W data yield shape parameters very close to the $n \sim 0.5$ value expected for isothermal distributions; for the F814W image,

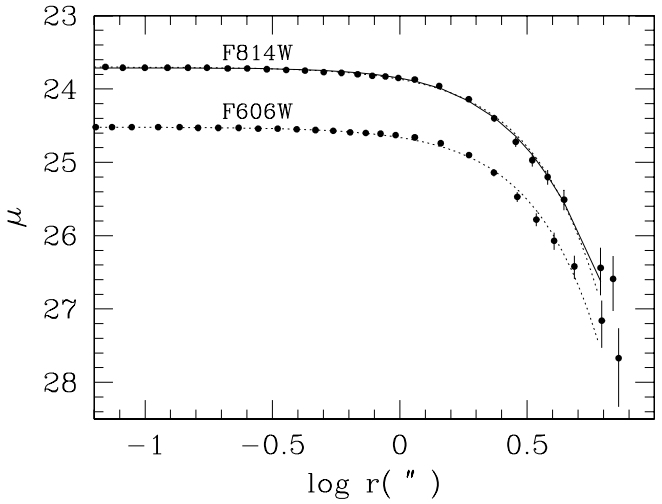

FIG. 8.—F814W and F606W surface brightness profiles derived by fitting elliptical contours to the smoothed images of the dSph galaxy. The data are plotted as a function of the geometric mean radius $r = (ab)^{1/2}$. The best-fitting King (1962) model, with $r_c = 2.6'' \pm 0.7''$ and $r_t = 10'' \pm 3''$, is shown as a solid line. The King (1962) model fit is excellent, with $\chi^2/\nu = 0.40$. The dashed lines denote the best fits to a Sérsic (1968) profile; see text for details.

$\Sigma_0 = 23.70 \pm 0.03$ mag arcsec^{-2}, $r_0 = 3.16'' \pm 0.16''$, and $n = 0.61 \pm 0.12$, while the F606W profile has $\Sigma_0 = 24.52 \pm 0.03$ mag arcsec^{-2}, $r_0 = 3.34'' \pm 0.06''$, and $n = 0.59 \pm 0.12$. Both fits (also plotted in Fig. 8) are only slightly worse than those for the King model ($\chi^2/\nu = 0.59$ and 0.63 for the F814W and F606W fits, respectively), but are still a very good match to the data.

We can also use the data of Figure 8 to compute the integrated magnitude of our galaxy. If we sum the flux contained within each elliptical isophote, then the total magnitude of the dwarf spheroidal is $F606W_{tot} = 20.56 \pm 0.05$ and $F814W_{tot} = 19.86 \pm 0.05$. These values are consistent with the F606W = 20.46 and F814W = 19.74 magnitudes obtained from simple photometry using an $11''$ circular aperture centered on the galaxy. To convert these magnitudes to V and I, we used the color transformations of Sirianni et al. (2005), and to obtain absolute magnitudes, we applied the distance and reddening values given in § 3.1; no additional corrections to our integrated magnitudes were required as our profiles extend to very faint surface brightnesses. The data imply that the dSph galaxy has a total absolute magnitude of $M_V = -10.6 \pm 0.2$ (and $M_I = -11.4 \pm 0.2$), where the error again includes both the uncertainties of the photometry and the distance.

3.5. *Comparison with Local Group dSph Galaxies*

Detailed observations in the Local Group demonstrate that dSph galaxies possess a variety of star formation histories and chemical abundances (Gallagher & Wyse 1994; Mateo 1998). This has been attributed to the effect of environment on their formation and evolution. If so, then the properties of such galaxies in dense clusters might be distinctly different from those of dSphs seen locally. Unfortunately, although a few dwarf galaxies have been studied in other nearby groups, such as the M81 system (Caldwell et al. 1998; Karachentsev et al. 2005; Da Costa 2005), very little is known about dSphs in rich clusters.

Figure 9 compares the observed central surface brightness, core radius, and metallicity of our Virgo dSph with the corresponding properties of dSph galaxies in the Local and M81 Groups. The most striking aspect of the figure is how normal our dSph appears.

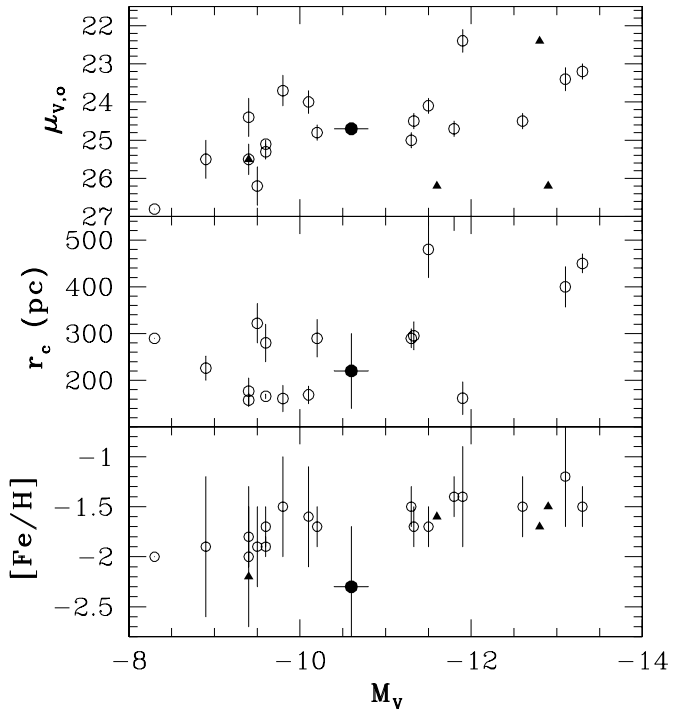

FIG. 9.—Comparison of the structural and chemical properties of the Virgo dSph (*filled circle*) with measurements for the dwarf spheroidals in the Local and M81 Groups (*open circles*). The top panel shows central surface brightness, the middle panel shows core radius, and the bottom panel shows metallicity, with the error bars representing the metallicity dispersion. The filled triangles denote measurements of faint dE/dSph galaxies in the Virgo Cluster from Caldwell (2006). The Local Group data come from the compilations of Irwin & Hatzidimitriou (1995), Grebel et al. (2003), and McConnachie & Irwin (2006), with additional information for individual dwarfs from Saviane et al. (1996), Palma et al. (2003), and Harbeck et al. (2005). The M81 dwarf data come from Caldwell et al. (1998). Note that the properties of the Virgo dwarf are completely consistent with those of dwarfs in these low-density systems.

The galaxy's structural parameters are similar to those of the Leo II and Ursa Minor dwarfs, i.e., typical of objects present in the local neighborhood. This result is consistent with the studies of Durrell (1997), Hilker et al. (2003), and Caldwell (2006), who also found no significant structural differences between the dwarfs of the Local Group and those of Virgo and Fornax. For comparison, the Virgo results from Caldwell (2006) are also plotted in Figure 9.

We reach a similar conclusion from the metallicity measurement of our dSph galaxy. Dwarf elliptical and spheroidal galaxies in the Local Group obey a well-established luminosity-metallicity relation (e.g., Smith 1985; Caldwell et al. 1992, 1998, 2006; Côté et al. 2000), where the more luminous galaxies are (on average) more metal-rich. This result, which is usually attributed to increased mass loss in systems with small potential wells (e.g., Dekel & Silk 1986), predicts the metallicity of our dSph galaxy fairly accurately. However, galaxies in clusters are expected to lose much of their mass to intracluster space via tidal encounters with other galaxies and with the cluster as a whole (e.g., Moore et al. 1996, 1998; Bekki et al. 2001). If our dSph had been exposed to these forces for any length of time, we would expect its metallicity to be more in line with that of a higher luminosity object. This does not appear the case; if anything, our galaxy's metallicity lies *below* the mean luminosity-metallicity relation. This suggests that most of the galaxy's original stars are still bound to the system, or perhaps the luminosity-metallicity relation differs in the cluster environment.

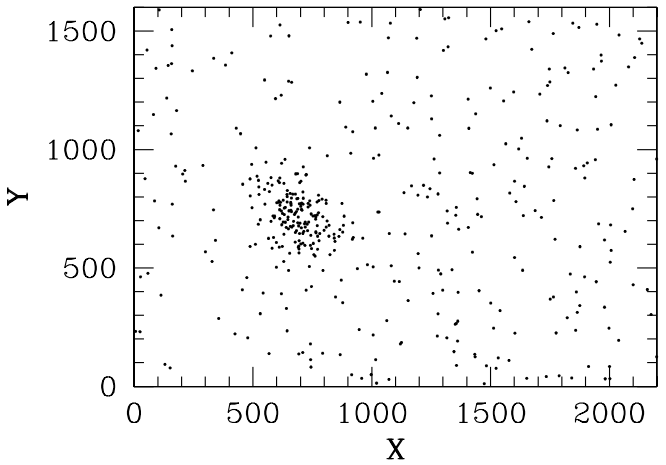

FIG. 10.—Spatial distribution (in pixels) for those stellar objects near our dwarf galaxy with the colors and magnitudes of metal-poor red giant stars (i.e., $0.4 < \mathrm{F606W} - \mathrm{F814W} < 1.3$ and $26.8 < \mathrm{F814W} < 28.0$). Each pixels represents $0.03''$, or $\sim$2.2 pc, at the distance of Virgo. There is no obvious evidence for the tidal shredding of the dwarf galaxy.

The structure of the galaxy appears to support this conclusion. Tidal features are often detected in dSph galaxies via photometric deviations from a King (1962) profile (e.g., Irwin & Hatzidimitriou 1995; Palma et al. 2003; Majewski et al. 2005). As Figure 8 demonstrates, our Virgo dwarf is well fit by a King model all the way down to $\mu_V \sim 27.5$ ($\mu_I \sim 26.5$), where the galaxy's surface brightness merges into that of the intracluster background (Williams et al. 2007a). Moreover, a plot of (x, y)-positions using only those stars with colors and magnitudes similar to those of the galaxy's RGB objects (i.e., $0.4 < \mathrm{F606W} - \mathrm{F814W} < 1.3$ and $26.8 < \mathrm{F814W} < 28.0$) reveals no obvious evidence for tidal distortion (Fig. 10). We note that our observations are not deep enough to see any low-level tidal disruption of this dSph galaxy; the large streams seen in the Coma and Centaurus Clusters are only visible at surface brightnesses below $\mu_V \sim 26$ (Trentham & Mobasher 1998; Gregg & West 1998; Calcáneo-Roldán et al. 2000), and the tails associated with the Local Group galaxies Carina and Ursa Minor are at $\mu_V \gtrsim 29$ (Palma et al. 2003; Majewski et al. 2005). Thus, we cannot unambiguously state whether the dSph galaxy has undergone any tidal stripping. Nevertheless, the metallicity arguments above suggest that the observed dSph is not the low-luminosity remains of a much more massive system (e.g., as expected in galaxy harassment scenarios).

Tidal threshing is not the only process that could affect dwarf galaxies in the cluster environment. In the Local Group, ram pressure stripping may be a prime factor in the evolution of dSph galaxies (Lin & Faber 1983; van den Bergh 1994; Grebel et al. 2003; Marcolini et al. 2003). Indeed, the *N*-body simulations of Mayer et al. (2006) suggest that both tides and ram pressure are needed to explain the properties of Local Group objects. If true, then the effects of intracluster gas should be magnified in the denser regions of the Virgo Cluster core. If low-luminosity dwarfs can barely hold onto their gas (and enrich themselves) in the Local Group, then Virgo dSphs should easily be stripped by the Virgo intracluster medium. The result would be a dSph galaxy much like those observed in the Local Group (as suggested by the structural similarities), but with less chemical enrichment and a very narrow red giant branch.

Our dSph does show some evidence for enhanced pressure stripping; as Figure 9 shows, the galaxy's mean metallicity is slightly less than that predicted from dSph observations in the Local and M81 Groups. However, our RGB photometry is not precise enough to test for self-enrichment. Local Group dwarfs typically have metallicity dispersions of $\gtrsim$0.3 dex (Mateo 1998). Our data, although consistent with a zero abundance spread, is best fit with an RGB color dispersion of $\sigma_{\mathrm{F606W-F814W}} = 0.05$ ($\sim$0.4 dex) and still admits a metallicity spread as great as $\sigma_{\mathrm{F606W-F814W}} = 0.09$ ($\sim$0.6 dex). Thus, while the data are suggestive, we cannot say for certain that the Virgo environment has had any additional effect on the dSph's chemical properties. Deeper photometric studies of other Virgo dSph galaxies would be very useful in ascertaining any differences between the chemical evolution of low-luminosity dwarf galaxies in clusters and those in the group environment.

4. DISCUSSION

From the analyses in § 3, it is clear that the dSph galaxy in our field lies in the Virgo cluster and appears relatively undisturbed by its surroundings. Its stellar population is very metal-poor ($[\mathrm{M/H}] \sim -2.3$) and old, with no indication of stars younger than $\sim$10 Gyr. In this sense it is similar to the purely old Local Group dSph galaxies of Ursa Minor and Draco. It is also similar to the dwarf galaxies recently observed by Caldwell (2006) in the Virgo Cluster core; their central surface brightnesses and metallicities are also included in Figure 9. They, too, obey the luminosity-metallicity relation for small galaxies and appear undisturbed by the cluster environment.

The appearance of such "pristine" old, low-luminosity dwarf galaxies within the Virgo Cluster begs a question: how do these objects last so long in the cluster? Small galaxies should be easy prey for the tidal forces associated with the cluster environment (Moore et al. 1998), and, indeed, the velocity distribution of Virgo dE galaxies supports the idea that at least some fraction of the cluster's dwarfs are the stripped remains of larger, late-type systems (e.g., Conselice et al. 2001). Furthermore, it is plausible that many of Virgo's metal-poor intracluster stars (Williams et al. 2007a) originated in such galaxies. Nevertheless, it seems clear that some dwarfs remain intact; perhaps these are dwarfs that have recently fallen into the cluster or have rather high M/L.

A weak constraint on the history of our dSph galaxy can be obtained from its observed tidal radius. From King (1962), the limiting radius of the galaxy should be

$$r_t = R_p \left[\frac{M_g}{M_C(3+\epsilon)} \right]^{1/3}, \tag{4}$$

where M_g is the mass of the galaxy, M_C is the mass of the cluster, R_P is the galaxy's pericluster radius, and ϵ is the eccentricity of the orbit. The mass of the galaxy can be obtained by analogy with Local Group objects; according to Mateo (1998), dwarf galaxies with $M_V \sim -10.6$ have mass-to-light ratios of $M/L_V \sim 10$, implying $M_g \sim 1.5 \times 10^7\ M_\odot$. The Virgo cluster mass is similarly obtainable from the X-ray observations of Nulsen & Böhringer (1995); their data give a core radius of 56 kpc, a mass per unit length of $12 \times 10^{10}\ M_\odot\ \mathrm{kpc}^{-1}$, and a total mass within 180 kpc (the projected cluster distance of the galaxy) of $2 \times 10^{13}\ M_\odot$. A value of $\epsilon \sim 0.5$ then excludes any orbit that extends into the inner $\sim$80 kpc of the cluster.

Of course, there are any number of ways to satisfy this condition. For instance, the dSph may just now be falling into Virgo for the first time. Cepheids, the planetary nebula luminosity function, the surface brightness fluctuation method, and the tip of the red giant branch all place the core of Virgo at a distance of between 14.5 and 17 Mpc (Freedman et al. 2001; Jacoby et al.

1990; Tonry et al. 2001; Jensen et al. 2003; Jerjen et al. 2004; Caldwell 2006). Our dSph distance estimate of 17.6 ± 1.4 Mpc is consistent with this range of values, but it also admits the possibility that the galaxy is slightly behind the main body of the cluster. If so, then the dSph's location may associate it with the infalling M86 system, which is ~3 Mpc beyond M87 (Böhringer et al. 1994; Jacoby et al. 1990; Tonry et al. 2001; Jerjen et al. 2004). If this scenario is correct, then our dwarf galaxy formed long ago in a smaller cluster/group, and the shredding of the galaxy is only now about to begin.

If the dwarf *did* originate and live much of its life in the cluster environment, then it would have to have a high mass to withstand the tidal forces of Virgo's densest regions. This would require a mass-to-light ratio that is much larger than the "normal" value of $M/L_V \sim 10$ observed in the Local Group. Cold dark matter (CDM) models do suggest that dwarf galaxies can form out of dark matter halos much more massive than dynamical measurements suggest (i.e., $M \sim 10^9$–$10^{10}\ M_\odot$; e.g., Stoehr et al. 2002; Hayashi et al. 2003; Kravtsov et al. 2004), and such objects would be able to resist tidal disruption. However, galaxies with large dark matter halos would not easily be stripped of their ISM by ram pressure or galactic winds. Mori & Burkert (2000) point out that while low-mass ($M \sim 10^6$–$10^7\ M_\odot$) objects will rapidly lose their gas to the intracluster medium, more massive systems are likely to hold on to at least some of their interstellar medium. As a result, their stellar populations should be younger and more metal-rich than their lower mass counterparts. While it is beyond the scope of this paper to investigate the precise masses and conditions under which early gas removal is expected, the old, metal-poor population of our dwarf spheroidal argues against the presence of a very massive dark halo. The existence of such a massive halo could, however, be tested via high-resolution spectroscopic observations with the next generation of large telescopes.

Unfortunately, our lack of knowledge about the dwarf's current location and orbital characteristics precludes our placing a strong constraint on its origin. While we have no data on the presence (or absence) of H I gas in the galaxy, that gas has certainly not created many new stars in the past ~8 Gyr. Thus, if gas were detected, it would not affect our basic conclusions.

5. SUMMARY

We report the discovery of a dwarf spheroidal galaxy (with $M_V = -10.6 \pm 0.2$) on deep ACS F606W and F814W images of an intracluster field in the Virgo Cluster. The distance to the galaxy is 17.6 ± 1.4 Mpc based on the location of its TRGB; this value is consistent with a location close to the core of the Virgo cluster, although we cannot rule out the possibility that this object is part of the M86 subcluster falling into Virgo from behind. The galaxy is clearly resolved into stars, and our observations extend more than a magnitude down its red giant branch.

We find that the galaxy is composed entirely of old stars (>8–10 Gyr) and is very metal-poor, with $[\mathrm{M/H}] = -2.3 \pm 0.3$. This metallicity is consistent with that expected for a galaxy of its luminosity; if anything, the galaxy lies slightly below the mean luminosity-metallicity relation. Thus, the object is not the remains of a larger galaxy that has been tidally stripped or harassed. Moreover, the dSph's structural properties are similar to those derived for dwarf galaxies in the Local and M81 groups, suggesting that many of the same physical processes that govern the formation and evolution of local dSphs also apply to this Virgo Cluster object. Based on this similarity, we suggest that our dSph galaxy is likely on its initial infall into the center of the cluster.

The authors would like to thank Tom Brown for assistance regarding dither patterns for the ACS observations and Chris Palma for reading an earlier version of this paper. Support for this work was provided by NASA grant GO-10131 from the Space Telescope Science Institute and by NASA through grant NAG5-9377. J. J. F. was supported by the NSF through grant AST-0302030, and T. v. H. was supported by NASA under grant NAG5-13070 issued through the Office of Space Science.

Facilities: HST (ACS)

REFERENCES

Armandroff, T. E., Da Costa, G. S., Caldwell, N., & Seitzer, P. 1993, AJ, 106, 986
Bekki, K., Couch, W. J., & Drinkwater, M. J. 2001, ApJ, 552, L105
Bellazzini, M., Ferraro, F. R., & Pancino, E. 2001, ApJ, 556, 635
Binggeli, B., Sandage, A., & Tammann, G. A. 1985, AJ, 90, 1681
Böhringer, H., Briel, U. G., Schwarz, R. A., Voges, W., Hartner, G., & Trümper, J. 1994, Nature, 368, 828
Brown, T. M., et al. 2005, AJ, 130, 1693
Busko, I. C. 1996, in ASP Conf. Ser. 101, Astronomical Data Analysis Software and Systems V, ed. G. H. Jacoby & J. Barnes (San Francisco: ASP), 139
Calcáneo-Roldán, C., Moore, B., Bland-Hawthorn, J., Malin, D., & Sadler, E. M. 2000, MNRAS, 314, 324
Caldwell, N. 2006, ApJ, 651, 822
Caldwell, N., Armandroff, T. E., Da Costa, G. S., & Seitzer, P. 1998, AJ, 115, 535
Caldwell, N., Armandroff, T. E., Seitzer, P., & Da Costa, G. S. 1992, AJ, 103, 840
Cioni, M.-R. L., van der Marel, R. P., Loup, C., & Habing, H. J. 2000, A&A, 359, 601
Cole, S., Lacey, C. G., Baugh, C. M., & Frenk, C S. 2000, MNRAS, 319, 168
Conselice, C. J., Gallagher, J. S., & Wyse, R. F. G. 2001, ApJ, 559, 791
Côté, P., Marzke, R. O., West, M. J., & Minniti, D. 2000, ApJ, 533, 869
Da Costa, G. S. 2005, in IAU Colloq. 198, Near-Fields Cosmology with Dwarf Elliptical Galaxies, ed. H. Jerjen & B. Binggeli (Cambridge: Cambridge Univ. Press), 35
Da Costa, G. S., & Armandroff, T. E. 1990, AJ, 100, 162
Dekel, A., & Silk, J. 1986, ApJ, 303, 39
Durrell, P. R. 1997, AJ, 113, 531
Durrell, P. R., Ciardullo, R., Feldmeier, J. J., Jacoby, G. H., & Sigurdsson, S. 2002, ApJ, 570, 119
Ferguson, H. C. 1989, AJ, 98, 367
Ferguson, H. C., Tanvir, N. R., & von Hippel, T. 1998, Nature, 391, 461
Ferrarese, L., et al. 2000, ApJ, 529, 745
Freedman, W. L., et al. 2001, ApJ, 553, 47
Gallagher, J. S., & Wyse, R. F. G. 1994, PASP, 106, 1225
Girardi, L., Bertelli, G., Bressan, A., Chiosi, C., Groenewegen, M. A. T., Marigo, P., Salasnich, B., & Weiss, A. 2002, A&A, 391, 195
Girardi, L., Bressan, A., Bertelli, G., & Chiosi, C. 2000, A&AS, 141, 371
Graham, A. W., & Driver, S. P. 2005, Publ. Astron. Soc. Australia, 22, 118
Grebel, E. K., Gallagher, J. S., & Harbeck, D. 2003, AJ, 125, 1926
Gregg, M. D., & West, M. J. 1998, Nature, 396, 549
Harbeck, D., Gallagher, J. S., Grebel, E. K., Koch, A., & Zucker, D. B. 2005, ApJ, 623, 159
Harris, W. E., Durrell, P. R., Pierce, M. J., & Secker, J. 1998, Nature, 395, 45
Hayashi, E., Navarro, J. F., Taylor, J. E., Stadel, J., & Quinn, T. 2003, ApJ, 584, 541
Hilker, M., Mieske, S., & Infante, L. 2003, A&A, 397, L9
———. 2005, in IAU Colloq. 198, Near-Field Cosmology with Dwarf Elliptical Galaxies, ed. H. Jerjen & B. Binggeli (Cambridge: Cambridge Univ. Press), 290
Irwin, M. J., & Hatzidimitriou, D. 1995, MNRAS, 277, 1354
Jacoby, G. H., Ciardullo, R., & Ford, H. C. 1990, ApJ, 356, 332
Jedrzejewski, R. I. 1987, MNRAS, 226, 747
Jensen, J. B., Tonry, J. L., Barris, B. J., Thompson, R. I., Liu, M. C., Rieke, M. J., Ajhar, E. A., & Blakeslee, J. P. 2003, ApJ, 583, 712
Jerjen, H., Binggeli, B., & Barazza, F. D. 2004, AJ, 127, 771
Karachentsev, I. D., Karachentseva, V. E., & Sharina, M. E. 2005, in IAU Colloq. 198, Near-Field Cosmology with Dwarf Elliptical Galaxies, ed. H. Jerjen & B. Binggeli (Cambridge: Cambridge Univ. Press), 295
Kauffmann, G., White, S. D. M., & Guideroni, B. 1993, MNRAS, 264, 201
King, I. 1962, AJ, 67, 471

Koekemoer, A. M., Fruchter, A. S., Hook, R. N., & Hack, W. 2002, in 2002 *HST* Calibration Workshop, Hubble after the Installation of the ACS and the NICMOS Cooling System, ed. S. Arribas, A. Koekemoer, & B. Whitmore (Baltimore: STScI), 337
Kravtsov, A. V., Gnedin, O. Y., & Klypin, A. A. 2004, ApJ, 609, 482
Kron, R. G. 1980, ApJS, 43, 305
Lee, M. G., Freedman, W. L., & Madore, B. F. 1993, ApJ, 417, 553
Lin, D. N. C., & Faber, S. M. 1983, ApJ, 266, L21
Madore, B. F., & Freedman, W. L. 1995, AJ, 109, 1645
Majewski, S. R., et al. 2005, AJ, 130, 2677
Marcolini, A., Brighenti, F., & D'Ercole, A. 2003, MNRAS, 345, 1329
Mateo, M. 1998, ARA&A, 36, 435
Mayer, L., Mastropietro, C., Wadsley, J., Stadel, J., & Moore, B. 2006, MNRAS, 369, 1021
McConnachie, A. W., & Irwin, M. J. 2006, MNRAS, 365, 1263
McConnachie, A. W., Irwin, M. J., Ferguson, A. M. N., Ibata, R. A., Lewis, G. F., & Tanvir, N. 2004, MNRAS, 350, 243
Méndez, B., Davis, M., Moustakas, J., Newman, J., Madore, B. F., & Freedman, W. L. 2002, AJ, 124, 213
Moore, B., Katz, N., Lake, G., Dressler, A., & Oemler, A. 1996, Nature, 379, 613
Moore, B., Lake, G., & Katz, N. 1998, ApJ, 495, 139
Mori, M., & Burkert, A. 2000, ApJ, 538, 559
Mouhcine, M., Ferguson, H. C., Rich, R. M., Brown, T. M., & Smith, T. E. 2005, ApJ, 633, 810
Mould, J., & Aaronson, M. 1982, ApJ, 263, 629
Neilsen, E. H., & Tsvetanov, Z. I. 2000, ApJ, 536, 255
Nulsen, P. E. J., & Böhringer, H. 1995, MNRAS, 274, 1093
Palma, C., Majewski, S. R., Siegel, M. H., Patterson, R. J., Ostheimer, J. C., & Link, R. 2003, AJ, 125, 1352
Phillipps, S., Parker, Q. A., Schwartzenberg, J. M., & Jones, J. B. 1998, ApJ, 493, L59
Rejkuba, M., Da Costa, G. S., Jerjen, H., Zoccali, M., & Binggeli, B. 2006, A&A, 448, 983
Sabatini, S., Davies, J., Scaramella, R., Smith, R., Baes, M., Linder, S. M., Roberts, S., & Tests, V. 2003, MNRAS, 341, 981
Sakai, S., Madore, B. F., & Freedman, W. L. 1996, ApJ, 461, 713
Saviane, I, Held, E. V., & Piotto, G. 1996, A&A, 315, 40
Schlegel, D. J., Finkbeiner, D. P., & Davis, M. 1998, ApJ, 500, 525
Sérsic, J.-L. 1968, Atlas de Galaxias Australes (Cordoba: Observatorio Astronomico)
Sirianni, M., Jee, et al. 2005, PASP, 117, 1049
Smith, G. H. 1985, PASP, 97, 1058
Stetson, P. B. 1987, PASP, 99, 191
———. 1992, in ASP Conf. Ser. 25, Astronomical Data Analysis Software and Systems, I., ed. D. M. Worral, C. Biemesderfer, & J. Barnes (San Francisco: ASP), 297
Stoehr, F., White, S. D. M., Tormen, G., & Springel, V. 2002, MNRAS, 335, L84
Tonry, J. L., Dressler, A., Blakeslee, J. P., Ajhar, E. A., Fletcher, A. B., Luppino, G. A., Metzger, M. R., & Moore, C. B. 2001, ApJ, 546, 681
Trentham, N., & Hodgkin, S. 2002, MNRAS, 333, 423
Trentham, N., & Mobasher, B. 1998, MNRAS, 293, 53
van den Bergh, S. 1994, ApJ, 428, 617
Williams, B. F., et al. 2007a, ApJ, 656, 756
———. 2007b, ApJ, 654, 835